Journal of ELECTRONIC MATERIALS, Vol. 42, No. 11, 2013
DOI: 10.1007/s11664-013-2776-8

Numerical Analysis of Current–Voltage Characteristics of LWIR nBn and *p*-on-*n* HgCdTe Photodetectors

M. KOPYTKO[1,2] and K. JÓŹWIKOWSKI[1]

1.—Institute of Applied Physics, Military University of Technology, 2 Kaliskiego St., 00-908 Warsaw, Poland. 2.—e-mail: mkopytko@wat.edu.pl

We performed numerical analysis of the current–voltage characteristics of long-wavelength infrared unipolar HgCdTe nBn photodetectors and compared those results with those of conventional *p*-on-*n* HgCdTe photodiodes. A computer program was applied to explain in detail the impact of the charge carrier generation and recombination processes on current densities. In our model the carrier diffusion, thermal generation–recombination, band-to-band tunneling, trap-assisted tunneling (via states located at mercury vacancies as well as dislocation cores), and impact ionization are included as potential limiting mechanisms. To validate the model, we compared the theoretical predictions with experimental data of high-quality *p*-on-*n* photodiodes published in the literature.

Key words: Generation–recombination processes, LWIR, HgCdTe, nBn, photodiode, photodetector

INTRODUCTION

Different long-wavelength infrared (LWIR, 8 μm to 12 μm) HgCdTe photodiode architectures have been fabricated that are compatible with backside- and frontside-illuminated hybrid focal-plane array technology. Generally, they can be divided into two families: *n*-on-*p* and *p*-on-*n* junctions. *n*-on-*p* junctions are fabricated in two different manners, using mercury vacancy doping and extrinsic doping. In *p*-on-*n* photodiodes, also called double-layer heterojunction structures, an absorber layer is *n*-type doped at 1×10^{15} cm^{-3} or less, and is sandwiched between the substrate and the highly arsenic-doped, wider-gap region.

In ideal *p*–*n* junction photodiodes the diffusion current is dominant, therefore their leakage current is very low and insensitive to the detector bias. However, in real devices many additional charge carrier generation and recombination (GR) mechanisms affect the dark current of HgCdTe photodiodes.[1] They arise from nonfundamental sources located in the absorber and cap layer, the depletion region, and the surface. Since radiative recombination, due to photon recycling, is not likely to limit the performance of properly designed infrared (IR) photodetectors,[2,3] only Auger as well as the Shockley–Read–Hall (SRH) mechanisms should be considered in HgCdTe as a main fundamental limit on detector performance.

The main leakage mechanisms of *p*–*n* junction photodiodes are generation in the depletion region, band-to-band tunneling (BtBT), trap-assisted tunneling (TAT), and impact ionization. Some of these are caused by structural defects in the *p*–*n* junction.[4,5] The TAT mechanism depends on the trap ionization energy, and BtBT depends on the energy gap. By increasing the energy gap in the junction region, tunneling currents might be significantly reduced. Such a solution is applied in the new type of IR detectors—the barrier IR detectors (BIRDs).

One of the ideas behind unipolar BIRDs—namely that a barrier could block one carrier type (electrons or holes) but allow unimpeded flow of the other as, for example, in the nBn structure—was proposed by Maimon and Wicks;[6] then, Ting et al.[7] used complementary barriers, i.e., a barrier for electrons and a barrier for holes at different depths, termed a complementary barrier IR device.

Figure 1 shows a comparison of schematics of the band structures of a reverse-biased *p*–*n* photodiode (Fig. 1a) and an nBn photodetector (Fig. 1b). The

(Received December 15, 2012; accepted September 7, 2013; published online October 8, 2013)

nBn detector can be considered as a hybrid of a photoconductor and a photodiode. It looks like a photodiode in part, except that the junction (space-charge region) is replaced by a wide-bandgap barrier (B), whereas the p^+-contact is replaced by an n^+-contact. When the detector is reverse biased, i.e., when a negative voltage is applied to the n^+ top contact, the unipolar barrier (B) blocks the flow of the majority-carrier (electron) current from the n^+ region, while allowing the collection of thermally and optically generated minority carriers (holes) from the absorber. Moreover, the extended bandgap in the junction area should contribute to a significant increase in the resistance of the detector by reducing the diffusion as well as generation–recombination currents, especially SRH and tunneling currents (both BtBT and TAT).

Figure 2 shows the schematic band structure of an Auger-suppressed unipolar barrier nBn detector. At the interface of the absorber and wide-bandgap, highly doped N^+ region, an exclusion junction is formed. Under reverse bias, holes are extracted from the absorber more effectively than they are injected by the exclusion junction, causing the hole concentration to drop significantly below its thermal equilibrium value. The electron concentration is also reduced below equilibrium to maintain charge neutrality in the absorber region. This causes a suppression of the Auger GR processes.

Currently, the $A_{III}B_V$ family of compounds plays a dominant role in the design of BIRD detectors due to the nearly zero band offset in the valance band. Type II superlattices (T2SLs) of InAs/GaSb with AlGaSb/T2SL barriers with tunneling and Auger GR process suppression have also shown potential capability for high-operating-temperature conditions, although short minority-carrier lifetimes ($\tau_{DIF}, \tau_{GR} < 10$ ns in the temperature range > 200 K) may impede the development of such T2SL IR devices.[8,9]

Even though HgCdTe does not exhibit a zero valance-band offset ("nested" type I heterojunction), the BIRD architecture was successfully adapted to the HgCdTe alloy, presenting technological advantages over *p–n* HgCdTe photodiodes [greatly simplifying the fabrication process of the *n*-type barriers and absorber and circumventing potential problems with *p*-type *in situ* doping in molecular beam epitaxy (MBE) growth].[10–14]

METHOD OF ANALYSIS

The first papers describing unipolar HgCdTe nBn photodetectors presented simple analyses carried out on the basis of a one-dimensional model.[10–13] In

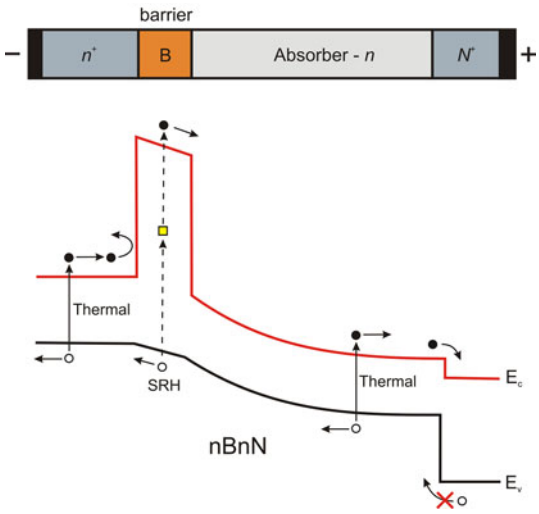

Fig. 2. Schematic band diagram of a reverse-biased nBnN detector.

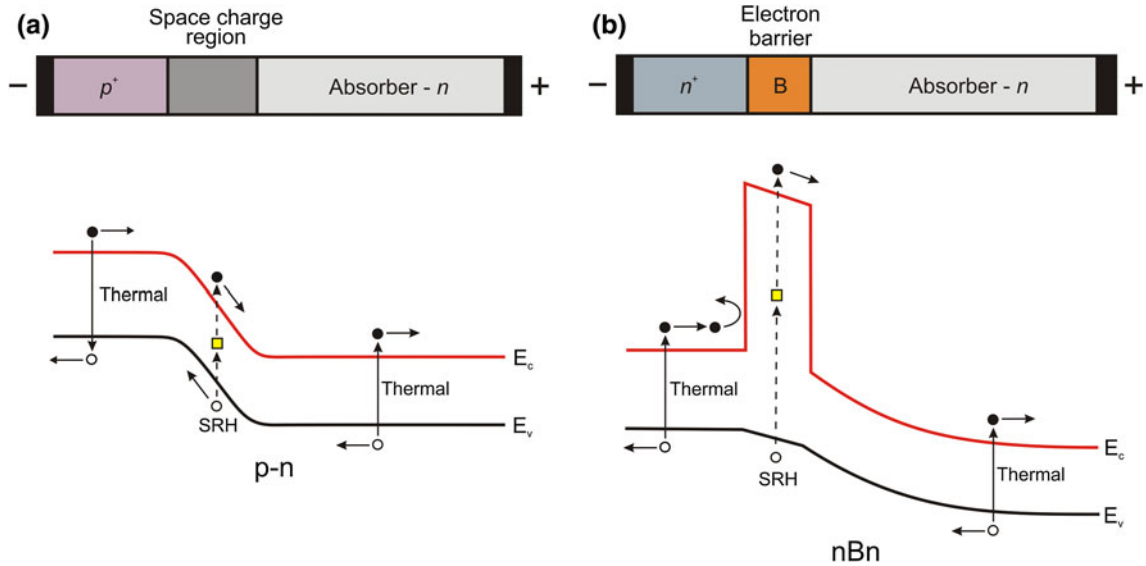

Fig. 1. Schematic band diagrams of a reverse-biased *p–n* photodiode (a) and nBn photodetector (b).

this work, we conducted advanced two-dimensional (2D) modeling for the mesa geometry structure shown in Fig. 3. Our computer program is based on solution of the set of transport equations comprising the continuity equations for electrons, holes, and photons, Poisson's equation, and the thermal conductivity equation. The advantage of this program compared with commercial programs lies in the possibility of modeling a wide spectrum of GR phenomena, including effects connected with structural defects. Two types of SRH center were considered: metal-site vacancies and dislocation-related centers. These two types of center are characterized by different ionization energies and capture cross-sections. The parameters were obtained by fitting of calculated results to experimental dark currents of high-quality photodiodes published in the available literature:[15]

- Vacancy parameters: Vacancy concentration of 1×10^{12} cm^{-3}, energy $0.75E_g$ above the valence band, electron and hole capture cross-sections $\sigma_n = \sigma_p = 5 \times 10^{-16}$ cm^2.
- Dislocation-related centers: The dislocation density was assumed to be the sum of the bulk and misfit dislocation densities. The bulk dislocation density was assumed to be composition independent and equal to 1×10^5 cm^{-2}. Misfit dislocation densities (in cm^{-2}) were calculated using the Yamamoto et al. expression[16]

$$N_{\mathrm{DIS}} = 5 \times 10^4 \nabla x, \tag{1}$$

where ∇x is the composition gradient in cm^{-1}. This expression assumes complete relaxation of misfit strain through the formation of dislocations.
- Dislocation-related SRH center parameters: Energy dislocation center at $0.32E_g$ above the valence band, electron and hole capture cross-sections $\sigma_n = \sigma_p = 5 \times 10^{-15}$ cm^2, one order of magnitude higher compared with those for vacancies.

Moreover, the model includes terms for interband tunneling, impact ionization, and effects connected with an electrical field. The influence of three other mechanisms (Frankel–Poole effect, TAT, and phonon-assisted tunneling) is also included. Detailed description can be found in our previous works.[4,5,17]

In this paper, we present the performance of a p–n junction and nBn-type LWIR $Hg_{1-x}Cd_xTe$ photodetectors operating at liquid-nitrogen temperature. The calculations were carried out for typical material parameters of the active layer for both types of device. An absorber layer about 15 μm thick was n-type doped with 1×10^{15} cm^{-3} donor concentration. The main advantage of this type of doping is that the n-type carrier concentration is easy to control in the 10^{15} cm^{-3} range using extrinsic doping, usually by indium or iodine (achieving p-type carrier concentration at this low level is difficult). The composition of the absorber was determined for devices with cutoff wavelengths equal to 9.7 μm at 78 K.

In the p-on-n photodiode, the highly doped p-type ($N_A = 5 \times 10^{16}$ cm^{-3}), wider-gap $Hg_{1-y}Cd_yTe$ ($y \approx x + 0.04$) cap was about 1 μm thick, whereas the nBn-type structures included a 1-μm-thick n-type-doped ($N_D = 5 \times 10^{16}$ cm^{-3}), wider-gap $Hg_{1-y}Cd_yTe$ ($y \approx x + 0.1$) cap layer. Between the cap layer and the absorber, the electron barrier was assumed to be p-type (B-p) with composition $x_B = 0.45$ and thickness of 50 nm. In the nBnN structure, the absorber is sandwiched between the barrier and a 1-μm-thick, highly doped ($N_D = 5 \times 10^{17}$ cm^{-3}), wider-gap $Hg_{1-y}Cd_yTe$ ($y \approx x + 0.1$) N^+ bottom layer.

The assumed composition and doping concentration profiles permit us to calculate the bandgap structure. Figure 4 shows the simulated energy band diagrams of unbiased and reverse-biased p-on-n HgCdTe photodiodes and nBn and nBnN HgCdTe photodetectors. In steady-state conditions, the interface of the wide-bandgap barrier and the absorber region consists of a valance-band barrier blocking the flow of minority carriers (holes) from the absorber (Fig. 4b, c; black dashed line). However, the holes from the absorber should be collected at the n^+ top contact. Therefore, optimal operation conditions require that the devices must be reverse biased, as shown in Figs. 1b and 2.

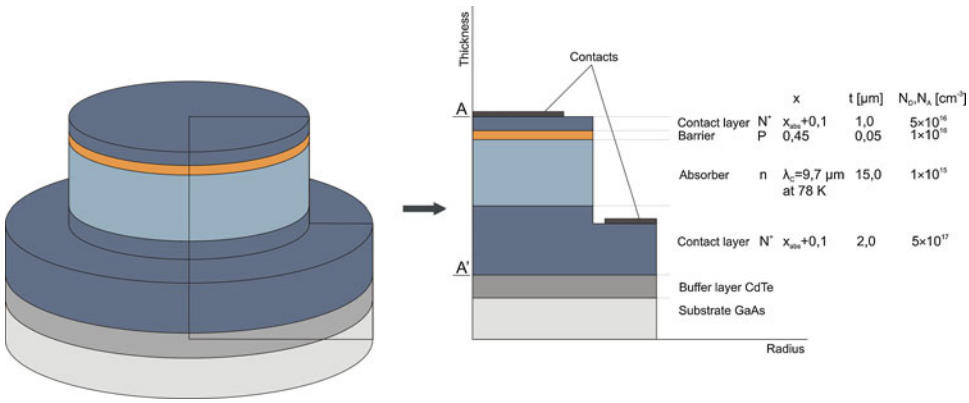

Fig. 3. Cross-section of the nBnN HgCdTe mesa structure. Device geometry: $r_1 = 34$ μm, $r_2 = 58$ μm.

RESULTS AND DISCUSSION

We begin our analysis with a comparison of the theoretical characteristics of the LWIR HgCdTe unipolar nBn photodetector with the *p*-on-*n* photodiode. Figure 5 shows current–voltage plots of both types of detector operating at 78 K. Experimental data for the *p*-on-*n* photodiode were taken from Ref. 15. We can see that, in the range of moderate voltage, the current densities are comparable for the nBn detector and *p*-on-*n* photodiode. Above 0.4 V reverse bias, the contribution of tunneling currents is very sensitive, especially for the *p*-on-*n* photodiode. This is mainly due to the TAT processes through dislocations at the p^+–n junction.

To show this, let us analyze Fig. 6a. In the absence of dislocations, the thermal generation rate in the junction region is lower than in the active region of the photodiode (solid red line). The presence of dislocations has a significant effect on the thermal generation. A high density of dislocations has little effect in most parts of the absorber, where the electric field is low, but significantly increases the thermal generation rate at the p^+–n junction (dashed red line). The electric field reduces the activation energy of traps associated with dislocations, thus the contribution of TAT currents through dislocation states is sensitive.

In the nBn detector, dislocations also increase the thermal generation at the barrier (Fig. 6b); however, the wide bandgap causes the activation energy of the traps to be high. The architecture of the nBn devices effectively eliminates the tunneling currents through trap states.

Now we compare the nBn and nBnN devices, whose theoretical current–voltage characteristics are shown in Fig. 5a and b, respectively. We can see that the nBnN device exhibits dark current density values two orders of magnitude lower than those observed for the nBn device. This significant decrease is the result of the effective Auger suppression mechanism due to the reduction of electron and hole concentrations. Under reverse bias, the holes are extracted from the absorber more effectively than they are injected by the exclusion junction, causing the hole concentration to drop significantly below its equilibrium value (Fig. 7).

However, dislocations cause a significant increase in current density (Fig. 5b). As in the case of the p^+–n junction, misfit dislocations significantly increase the field trap-assisted SRH generation at the n–N^+ junction (Fig. 6c) where the electrical field is large. The n–N^+ junction region becomes the main contributor to the resulting thermal generation and dark current above 0.1 V reverse bias.

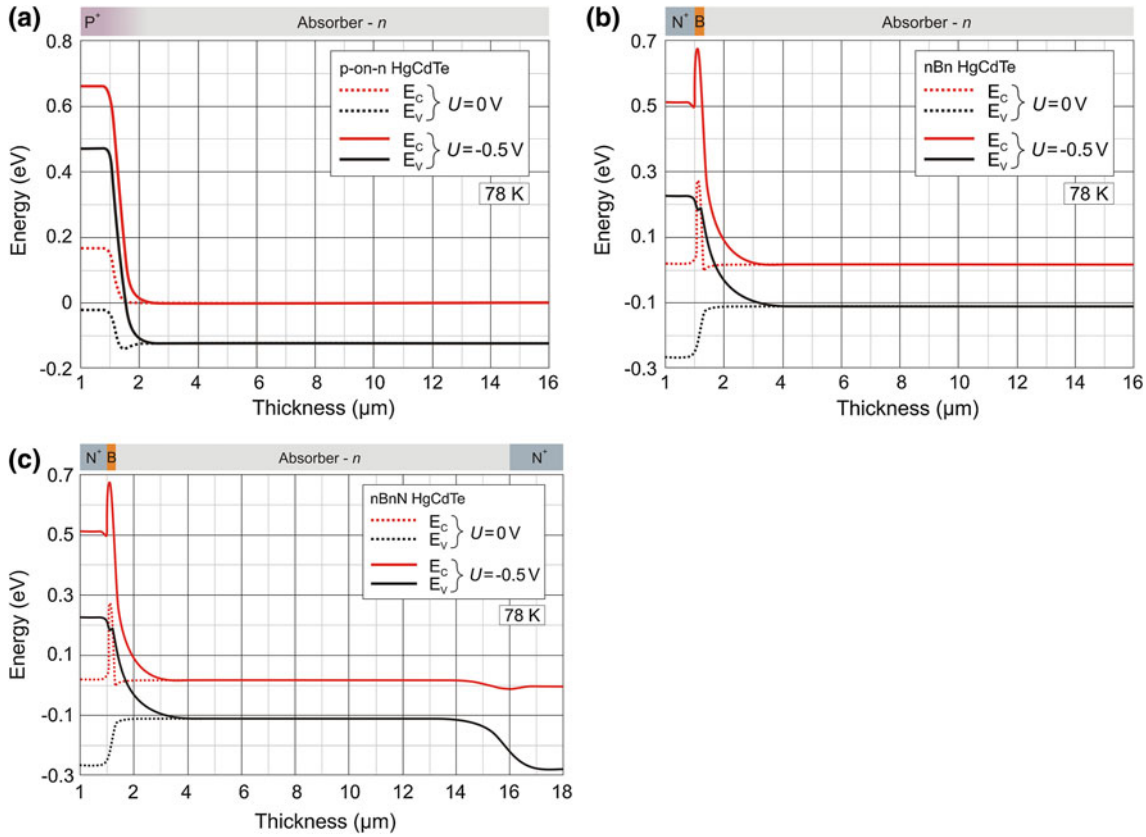

Fig. 4. Simulated energy band diagrams of unbiased and 0.5 V reverse-biased *p*-on-*n* HgCdTe photodiode (a), nBn HgCdTe (b) and nBnN HgCdTe (c) photodetectors operating at 78 K.

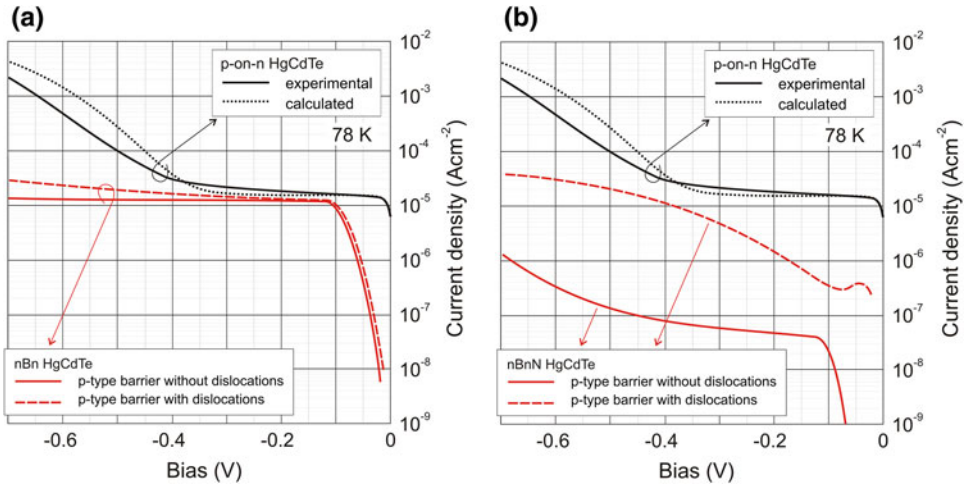

Fig. 5. Current–voltage characteristics of LWIR HgCdTe nBn (a) and nBnN^{+} (b) photodetectors operating at 78 K compared with experimental data[15] and theoretical predictions of a *p*-on-*n* HgCdTe photodiode.

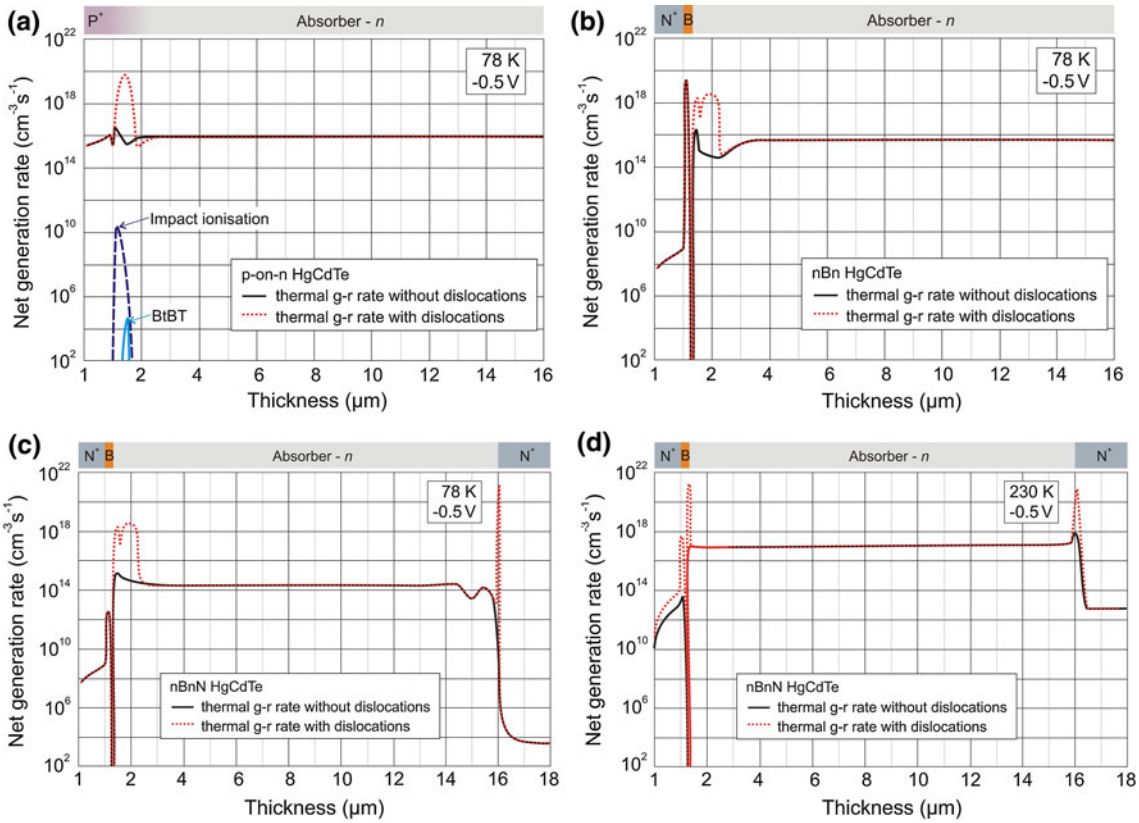

Fig. 6. Spatial distribution of the thermal generation rate of a 0.5 V reverse-biased *p*-on-*n* HgCdTe photodiode (a), and nBn (b) and nBnN (c) HgCdTe photodetectors operating at 78 K, and nBnN HgCdTe photodetector operating at 230 K (d). The dashed line shows the case with the influence of mismatch dislocations.

In the case of detectors optimized for operation with a Peltier cooler (about 230 K), the impact of misfit dislocations is not as significant. Figure 8 shows calculated curves for both temperatures: 78 K (red lines) and 230 K (blue lines), obtained with and without assumption of dislocations. Misfit dislocations also increase the field trap-assisted SRH generation at the n–N^{+} junction (Fig. 6d), although by only about one order of magnitude, while at 78 K this increase is much higher: about seven orders of magnitude (Fig. 6c).

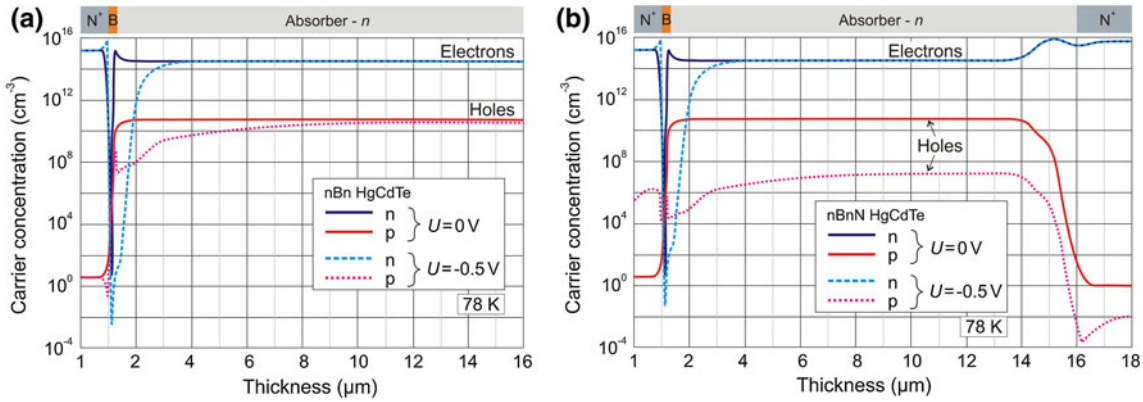

Fig. 7. Spatial distributions of electron and hole concentrations at equilibrium and at 0.5 V reverse biasing for LWIR nBn (a) and nBnN (b) HgCdTe photodetectors operating at 78 K.

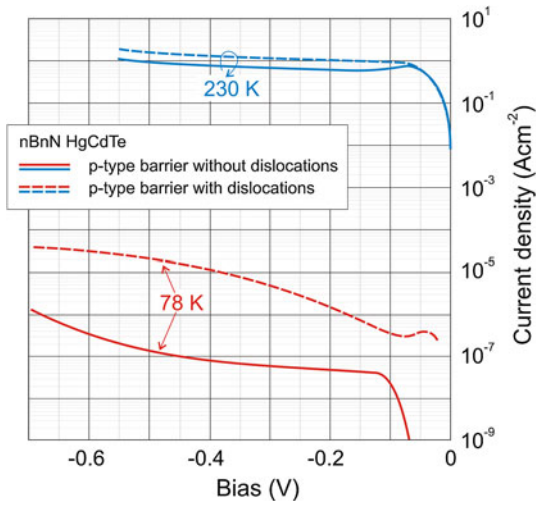

Fig. 8. Current–voltage characteristics of a LWIR HgCdTe nBnN photodetector operating at 78 K (red lines) and 230 K (blue lines).

CONCLUSIONS

The performance of LWIR unipolar nBn-type HgCdTe photodetectors and *p*-on-*n* photodiodes was investigated by computer simulations compared with experimental data. The work indicated that the new type of IR detectors might be a promising alternative to traditional *p*–*n* junction devices. While field-enhanced TAT via traps located at dislocation cores as well as mercury vacancies seems to be the most important mechanism of dark current generation at *p*–*n* photodiodes, the appropriate architecture of barrier-type detectors eliminates these problems. The extended bandgap in the junction area should reduce the diffusion and SRH GR currents.

ACKNOWLEDGEMENTS

The work has been completed and undertaken thanks to the financial support of the Polish National Science Center as research Project No. DEC-2011/03/D/ST7/03161.

OPEN ACCESS

REFERENCES

1. A. Rogalski, K. Adamiec, and J. Rutkowski, *Narrow-Gap Semiconductor Photodiodes* (Bellingham: SPIE Press, 2000).
2. K. Jóźwikowski, M. Kopytko, and A. Rogalski, *Opt. Eng.* 50, 061003 (2011).
3. K. Jóźwikowski, M. Kopytko, and A. Rogalski, *J. Electron. Mater.* 41, 2766 (2012).
4. K. Jóźwikowski, M. Kopytko, A. Rogalski, and A. Jóźwikowska, *J. Appl. Phys.* 108, 074519 (2010).
5. K. Jóźwikowski, M. Kopytko, and A. Rogalski, *Bull. Pol. Acad. Sci.* 58, 523 (2010).
6. S. Maimon and G. Wicks, *Appl. Phys. Lett.* 89, 151109 (2006).
7. D.Z. Ting, C.J. Hill, A. Soibel, J. Nguyen, S.A. Keo, J.M. Mumolo, M.C. Lee, B. Yang, and S.D. Gunapala, *SPIE Proc. Ser.* 7419, 74190B (2009).
8. P. Martyniuk, J. Wrobel, E. Plis, P. Madejczyk, A. Kowalewski, W. Gawron, S. Krishna, and A. Rogalski, *Semicond. Sci. Technol.* 27, 055002 (2012).
9. J. Wróbel, P. Martyniuk, E. Plis, P. Madejczyk, W. Gawron, S. Krishna, and A. Rogalski, *SPIE Proc. Ser.* 8353, 16 (2012).
10. S. Velicu, J. Zhao, M. Morley, A.M. Itsuno, and J.D. Philips, *SPIE Proc. Ser.* 8268, 82682X (2012).
11. A.M. Itsuno, J.D. Philips, and S. Velicu, *J. Electron. Mater.* 41, 2886 (2012).
12. A.M. Itsuno, J.D. Phillips, and S. Velicu, *J. Electron. Mater.* 40, 1624 (2011).
13. A.M. Itsuno, J.D. Phillips, A.S. Gilmore, and S. Velicu, *SPIE Proc. Ser.* 8155, 81550J-1-5 (2011).
14. P. Martyniuk and A. Rogalski, *Solid State Electron.* 80, 96 (2012).
15. O. Gravrand, L. Mollard, C. Largeron, N. Baier, E. Deborniol, and Ph Chorier, *J. Electron. Mater.* 38, 1733 (2009).
16. Y. Yamamoto, Y. Miyamoto, and K. Tonikawa, *J. Cryst. Growth* 72, 270 (1985).
17. K. Jóźwikowski, A. Jóźwikowska, M. Kopytko, A. Rogalski, and L.R. Jaroszewicz, *Infrared Phys. Technol.* 55, 98 (2011).